

Research Paper

Comparison of equilibrium-based and kinetics-based models for evaluating the impact of hydrogen carrier reforming on SOFC system

Clyde-Theodore N. Batista^a, Kazeem Ayodeji Mohammed^a, Amirpiran Amiri^{a,*}, Neda Azimi^b, Robert Steinberger-Wilckens^c

^a Energy and Bioproducts Research Institute (EBRI), School of Engineering and Applied Science, Aston University, Birmingham B4 7ET, United Kingdom

^b CFD Research Center, Department of Chemical Engineering, Razi University, Kermanshah, Iran

^c School of Chemical Engineering, University of Birmingham, Edgbaston, Birmingham B15 2 TT, United Kingdom



ARTICLE INFO

Keywords:

SOFC
Hydrogen
Fuel Reforming
Kinetics model
Equilibrium model

ABSTRACT

This paper evaluates the computational risks of using Equilibrium-Based Models (EBMs) and Kinetics-Based Models (KBM) interchangeably for simulating the external reformer in Solid Oxide Fuel Cell (SOFC) Balance of Plant (BoP). Various reforming processes, including steam reforming, partial oxidation, and autothermal reforming of hydrocarbons are assessed. The study systematically investigates the effect of reformers operating parameters, such as temperature, pressure, steam-to-carbon ratio, and oxygen-to-carbon ratio, on SOFC performance captured by EBM and KBM. In contrast to EBM, the KBM consistently provided a more detailed and accurate measures of system behaviour. This is more evident, especially under conditions where reaction kinetics play a crucial role, such as in high-pressure scenarios or significant variations in the steam-to-carbon ratio. The KBM captured the details of reaction kinetics and mass transfer limitations that the EBM, with its inherent assumption of near-instantaneous equilibrium, could not fully replicate. While EBM is computationally effective for minimising modelling complexity/time at the system level, it has limitations in scenarios that require detailed reaction kinetics due to the nature of reaction or fuel mixture. EBM and KBM results deviations are quantified to identify regions where these risks are either significant or tolerable.

1. Introduction

SOFCs are appealing for diverse applications such as automotive, aviation, marine, power generation, and residential due to their high efficiency, lack of moving parts, fuel flexibility, and capacity range [1]. Introducing cogeneration and optimising fuel and oxidant use can further enhance efficiency; for instance, using exhaust heat in a combined heat and power (CHP) system can raise SOFC efficiency to over 90 % [2–4]. Despite their advantages, SOFC systems face challenges in balancing performance and durability, leading to trade-offs that limit widespread adoption [5]. Most research has focused on material and catalyst issues [6,7], but system-level improvements are crucial for longevity, as SOFC health depends on BoP design and performance. For example, an external fuel reformer significantly impacts SOFC efficiency and lifespan, meaning even a well-designed SOFC may underperform in a suboptimal BoP.

Fuel sustainability and reliability are key system-level challenges, especially when using hydrogen carriers like ammonia and methane to

ensure long-term SOFC performance [8,9]. The variety of reforming routes (SR, POX, ATR, DR) and models introduces risks to the reliability of multi-fuel system simulations. Several studies have compared internal and external reforming in SOFC systems. Chitsaz et al. [10] found that internal reforming reduces CO₂ emissions by 1.4 % compared to external reforming. Chen et al. [11] reported better performance with internal reforming at high fuel utilisation, while external reforming enhances stack efficiency and reduces size at lower utilisations. Cocco and Tola [12] showed that external reforming is preferable with methanol to reduce system temperatures. Limited studies address reforming effects on SOFC and BoP efficiency; however, Liese et al. [13] found 8 % higher efficiency with internal reforming, and Authayanun et al. [14] simulated biogas reforming to assess S/C ratio, temperature, and pressure effects on SOFC performance. Liso et al. [15] compared POX and SR performance in SOFCs fuelled by natural gas.

With numerous fuel options and operating conditions for SOFCs, identifying optimal fuel mixtures, reforming routes, and conditions is challenging. This paper addresses the main gaps, including the need for a systematic and efficient evaluation strategy within the SOFC BoP. It

* Corresponding author.

E-mail address: a.p.amiri@aston.ac.uk (A. Amiri).

<https://doi.org/10.1016/j.enconman.2025.119733>

Received 30 November 2024; Received in revised form 2 March 2025; Accepted 9 March 2025

Available online 15 March 2025

0196-8904/© 2025 The Author(s). Published by Elsevier Ltd. This is an open access article under the CC BY license (<http://creativecommons.org/licenses/by/4.0/>).

Nomenclature		ΔV_P	Voltage changes as a function of pressure (V)
C_i	Molar flow rate (mol/hr)	ΔV_T	Voltage changes as a function of temperature (V)
I_c	Current density (mA/cm ²)	<i>Greek letters</i>	
K	Voltage variation constant (-)	η	The gross AC efficiency (-)
LHV_{Fuel}	Lower heating value (J/mol)	<i>Acronyms</i>	
$n_{H_2, equivalent}$	Equivalent hydrogen flow rate (mol/hr)	ATR	Auto thermal reforming
$n_{Fresh fuel}$	Fresh fuel flow rate (mol/hr)	BoP	Balance-of-plant
P	Operating pressure (bar)	CHP	Combined heat and power
P_{ref}	Reference-operating pressure (bar)	DR	Dry reforming
P_{O_2}	Average oxygen partial pressure at the cathode (bar)	HC	Hydrocarbon
P_{O_2ref}	Average oxygen partial pressure at the cathode under reference condition (bar)	O/C	Oxygen-to-carbon ratio
T	Operating temperature (K)	PFD	Process flow diagram
U_f	Fuel utilisation (-)	POX	Partial oxidation
V	Cell voltage (V)	S/C	Steam-to-Carbon ratio
V_{ref}	Reference voltage (V)	SOFC	Solid oxide fuel cell
ΔV_{Anode}	Anode voltage change (V)	SR	Steam reforming
$\Delta V_{Cathode}$	Cathode voltage change (V)		

Table 1
The reforming reactions rate equations and parameters.

Reactions	Rate equation	Reference
$SR C_n H_m + n H_2 O \leftrightarrow \left(n + \frac{1}{2}m\right) H_2 + n CO$	$-r_{HC} = \frac{k_0 e^{-\frac{E}{RT}} P_{HC}^\alpha P_{H_2O}^\beta}{1 + \theta P_{H_2}^\delta}$	[18,19]
$POX C_n H_m + \left(\frac{1}{2}n\right) O_2 \leftrightarrow \left(\frac{1}{2}m\right) H_2 + n CO$	$\ln(r_{HC}) = \ln(k_0) - \frac{E_a}{R} \left(\frac{1}{T}\right) + \alpha \ln(P_{HC}) + \beta \ln(P_{O_2})$	[20,21]
$ATR C_n H_m + \left(\frac{1}{2}n\right) H_2 O + \left(\frac{1}{4}n\right) O_2 \leftrightarrow \left(\frac{1}{2}n + \frac{1}{2}m\right) H_2 + n CO$	Combination of SR and POX kinetics	[19]
$wgs CO + H_2 O \leftrightarrow CO_2 + H_2$	$k^{-1} = 299377 \text{ L/mol}\cdot\text{s (M)}$ $E = 47.4 \text{ kJ/mol}$	[19]

Table 2
Input data for steam reforming route [19].

Fuel	T (°C)	k_0 (mol/kPa ^{$\alpha+\beta$} .m ² .hr)	E_a (kcal/mol)	α	β	δ
CH ₄	623–673	152.5	14.3	0.96	-0.17	0.25
C ₂ H ₆	583–623	30,488	19.2	0.95	-0.46	0.38
C ₃ H ₈	583–623	2.1428×10^{14}	45.3	0.93	-0.53	0.86

leverages the extensive use of both equilibrium and kinetic models from the literature in simulating reforming routes to improve SOFC viability for clean energy.

This paper addresses the unquantified impact of reforming models on SOFC system behaviour by proposing a system-level approach to assess SR, POX, and ATR routes using both equilibrium-based (EBM) and kinetic-based models (KBM). Leveraging commercial thermodynamics databases available in commercial process simulators (Aspen Plus), this method enables evaluation of various fuels and mixtures, contributing by (i) filtering fuel mixtures for optimal performance and identifying promising reforming routes, and (ii) determining the most suitable reforming model for real-life BoP conditions.

The paper is structured as follows: A base BoP simulation was

Table 3
Input data for partial oxidation route.

Fuel	T (°C)	k_0 (cm ³ /mol.s ^{$\alpha+\beta$})	E_a (kcal/mol)	α	β	Reference
CH ₄	697–780	1.25×10^8	26.96 ± 0.2	1.00 ± 0.05	0.0 ± 0.05	[22]
C ₂ H ₆	473–543	3.49×10^5	19.14 ± 0.2	1.0 ± 0.1	0.0 ± 0.1	[23]
C ₃ H ₈	423–463	1.20×10^5	23.00 ± 0.2	1.1 ± 0.05	-0.6 ± 0.1	[23]

developed in Aspen Plus and validated with literature data [16,17]. Due to the Lack of a built-in SOFC model, semi-empirical equations were combined with conventional reactor models. Given these constraints, this study adopts an external reforming approach, allowing for independent process simulation of fuel conversion before entering the SOFC anode. This ensures the system will be capable to test various hydrogen carriers reforming while mitigating carbon deposition risks, thermal stress, and operational instability. BoP modifications were then applied to assess SR, POX, and ATR effects on SOFC performance, with dominant parameters specific to each route evaluated using both EBM and KBM to quantify modelling assumption impacts.

2. Modelling and simulation

2.1. The base simulation and validation

Inspired by Zhang et al. [16], a system model was developed in Aspen Plus to capture various external reforming routes performances. The reforming rate equations and input parameters used for the KBM, and the process flow diagram (PFD) for the base case are presented in Table 1, Table 2, Table 3 and Fig. 1, respectively.

Where θ ($= 1.0 \text{ kPa}^{-\delta}$ [19]) represents the empirical inhibition factor

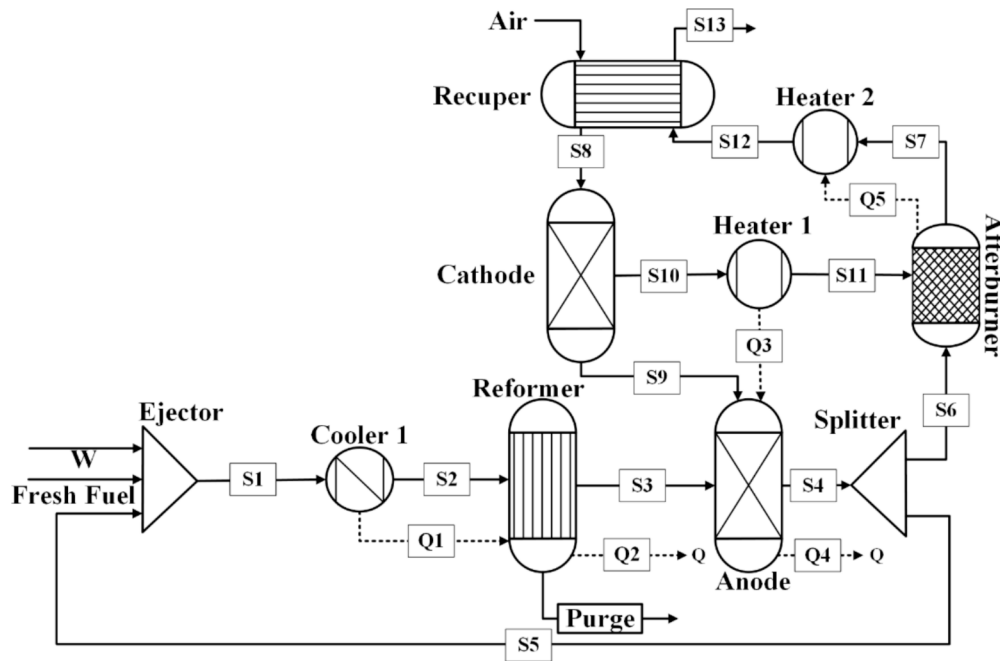


Fig. 1. Base case PFD.

Table 4

Iterative SOFC performance equations using BoP data [16,28].

Set	Equations set	No.	Description / Reference
Cell voltage	$V = V_{ref} + \Delta V_p + \Delta V_T + \Delta V_{anode} + \Delta V_{cathode}$	(1)	–
Voltage variation function of pressure	$\Delta V_p(mV) = 59 \times \log(P/P_{ref})$	(2)	1 atm < P < 10 atm [23].
Voltage changes as a function of temperature	$\Delta V_T(mV) = K \times (T - T_{ref}) \times I_c$	(3)	K is T dependent [23].
The voltage difference due to a change in fuel utilisation	$\Delta V_{anode}(mV) = 172 \times \log\left[\frac{(P_{H_2}/P_{H_2O})}{(P_{H_2}/P_{H_2O})_{ref}}\right]$	(4)	–
The voltage variation due to a change in oxidant utilisation	$\Delta V_{cathode}(mV) = 92 \times \log\left(\frac{P_{O_2}}{P_{O_2,ref}}\right)$	(5)	0.16 < P _{O₂} / P _{O_{2,ref}} < 0.2 [12].
The equivalent hydrogen flow rate	$n_{H_2, equivalent}(mol/hr) = (0.018655 \times I) / U_f$	(6)	–
The fresh fuel flow rate	$n_{freshfuel}(mol/hr) = \frac{n_{H_2, equivalent}}{C_{H_2} + C_{CO} + 4C_{CH_4} + 7C_{C_2H_6} + \dots}$	(7)	–
The gross AC efficiency	$\eta = \frac{P}{n_{freshfuel} \times LHV_{fuel}}$	(8)	–

that accounts for the suppressing effect of H₂ on the reforming reaction rate.

Since Aspen Plus does not offer a built-in SOFC model, an iterative computation approach was employed to simulate the unit deploying equations presented in Table 4. The model adopts an experimental curve published in the Fuel Cell Handbook [24] as the reference curve to define the reference voltage (V_{ref}) under the specified operating conditions (inlet fuel composition: 67 % H₂, 22 % CO, 11 % H₂O, fuel utilization (U_f) = 85 %, air utilization (U_a) = 25 %, T = 1000 °C, and P = 1 bar). The cell voltage is calculated as the sum of the reference voltage and voltage variations due to pressure (ΔV_p), temperature (ΔV_T), anode reaction (ΔV_{anode}), and cathode reaction ($\Delta V_{cathode}$), as detailed in Equations (1) to (5) in Table 4. Alternative methods have also been developed and successfully applied for modelling objectives such as fuel cell thermal management [25–27]. As adopted from Zhang et al.'s [16] model, a splitter recirculates a fraction of the anode exhaust to the ejector, mixing with fresh fuel to preheat it and supply steam for external reforming before entering the reformer. The split ratio is dynamically set in Aspen Plus via a Design-spec function to maintain a desired steam-to-carbon (S/C) ratio of 2.5 for base case and for scenarios where it is not specified, while another Design-spec function calculates the required fresh fuel inlet pressure (P_{fresh}) for anode gas recycling. The flowsheet

data served as inputs for the SOFC equation set in an interactive spreadsheet calculation. To initiate the computation, the process parameters and conditions were first guessed, for a 120 kW base case system. The voltage, and current were estimated using Equation (1) and P/V, respectively. The fresh fuel, subsequently, was estimated by using Equations (6) and (7). The new voltage value was then computed using Equations (1) to (8). Subsequently, the power was calculated and compared to the targeted power. If these two power values demonstrated good agreement within a specified tolerance, the computation could be terminated. Otherwise, the iteration process continued until the error met the tolerance.

The results of the base simulation were compared to the data provided by Zhang et al. [16] and Doherty et al. [17], and a good agreement was observed (Table 5). It should be noted that the fuel feedstock used in [16,17] differed slightly from the one used in this study. Specifically, minor butane present in the fuel was removed to minimise the error that its reaction kinetics uncertainty may cause in a rate-based simulation.

The adjustment in the fuel composition could contribute to the small deviations observed in Table 5, particularly in the parameters directly influenced by the reforming process, such as the reformer methane conversion, reformer temperature, the anode inlet and exhaust gas compositions. For instance, the removal of butane likely led to slight

Table 5

Base case simulation validation against literature data.

Parameters	Ref. [13]	Ref. [14]	This work	Average deviation %
Voltage (V)	0.70	0.68	0.70	1.28
Current density (mA/cm ²)	1780	1828	1776	1.24
Reforming temperature (°C)	536	535	531	0.37
Cathode inlet temperature (°C)	821	823	821	0.11
Reformer methane conversions (%)	25.9	25.0	23.3	3.86
Reformer C ₁₊ conversions (%)	100	100	100	0.00
<u>Anode inlet molar composition (%)</u>	10.1	10.4	11.3	4.40
CH ₄	27.0	26.9	26.5	0.75
H ₂	27.9	27.8	27.6	0.40
H ₂ O	5.60	5.60	5.30	2.42
CO	23.1	23.1	23.0	0.19
CO ₂	6.20	6.20	6.30	0.71
N ₂				
<u>Anode exhaust gas molar composition (%)</u>	11.650.97.4024.95.10	11.650.97.4024.95.10	11.251.47.1025.25.10	1.550.441.830.530.00
CH ₄				
H ₂				
H ₂ O				
CO				
CO ₂				
N ₂				
<u>Cathode exhaust gas molar composition (%)</u>	82.3	82.3	82.3	0.00
O ₂				
N ₂				
Gross AC efficiency (LHV)	52.0	51.3	52.2	0.69

changes in the reformer and anode gas compositions, contributing to the reported deviations of 3.86 % in methane conversion and 2.42 % in CO composition at the anode inlet which could stem slight alteration of the overall reaction dynamics and heat balance within the system. Despite these deviations, the overall agreement with the literature data remains strong, indicating that the simulation assumptions were reasonable and that the results are reliable.

2.2. Simulation platform upgrading

To enhance the accuracy and realism of the fuel reforming subsystem in the BoP, a rigorous and flexible approach was adopted to replace the equilibrium-based SR model used in the base simulation. The objective was to provide reactions inputs to capture the real-life characteristics of the reforming process. As a result, it became possible to simulate each reforming route using EBM and KBM. This platform enables the analysis of numerous system-level scenarios that are technically important. Thanks to Aspen process analysis tools, an efficient computation of these scenarios became feasible. Each reforming route has its specific parameters, such as the S/C ratio for SR and the O/C ratio for POX. The upgraded platform proved to be highly effective and efficient in investigating a wide range of parameters within a single BoP with minimal modifications. Aspen Plus allows specifying a reference temperature (T_0) for KBM, calculated as the average temperature from the recommended range in References [19,22], and [23] for each kinetic parameter. This ensures model accounts for temperature variability, making the parameters applicable across different temperatures.

With reference to Fig. 2, R-Equil and R-Plug reactors models, operating adiabatically, were deployed to simulate the EBM-based and KBM-based SR process simulation, respectively. The reformer geometry parameters reported by Doherty et al. [17] were considered as constant parameters for all the studied cases. This assumption is reasonable given the comparative nature of this study.

Fig. 3(a) and (b) show the PFDs for the EBM and KBM used in the simulation of BoP with a POX pre-reformer.

As POX is an exothermic reaction, the heat integration configuration is considerably different compared to the system with an endothermic SR subsystem. The stoichiometric reaction for POX was used in the reactor block, along with their respective operating conditions.

The stream 'O' shown in both configurations (Fig. 3) was added as an

oxidant to provide the oxygen feedstock, replacing the steam stream (W). The Design Specification tool was used to adjust the O/C ratio. Fig. 4(a) and Fig. 4(b) show the PFDs for the EBM and KBM, respectively, used in the simulation of the system with an ATR pre-reformer where steam and oxygen streams are added simultaneously.

3. Results and discussion

3.1. Steam reforming route

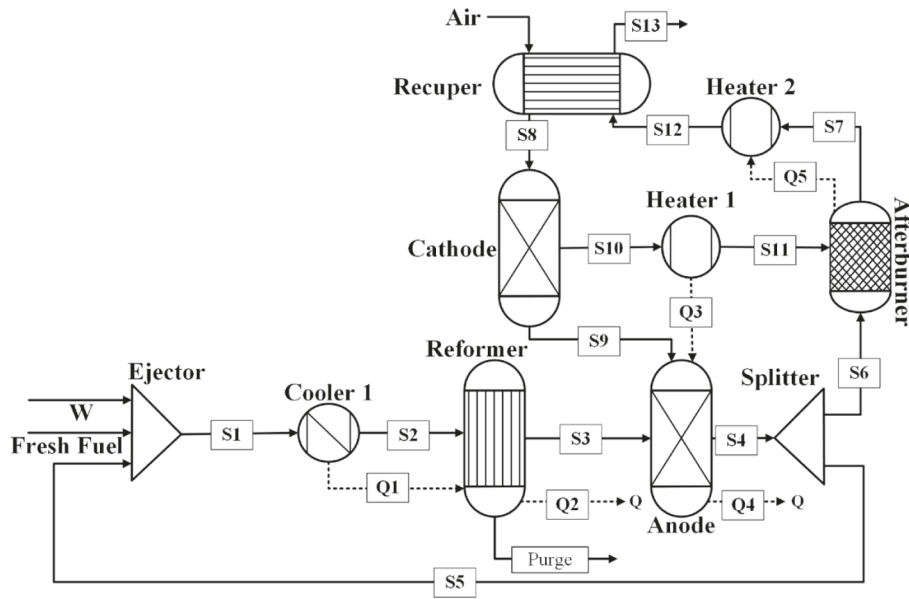
The input parameters for the SOFC model were obtained from Zhang et al. [16], except that the cell operating temperature is set to 910 °C instead of the 1000 °C used by Zhang et al. [16].

Fig. 5 illustrates the impact of the reformer temperature on the SOFC operating parameters. As observed, both the EBM and KBM models predict a discernible increase in voltage, rising from 0.6 V to 0.74 V and from 0.76 V to 0.80 V, respectively, which corresponds with variations in partial pressures, particularly the water partial pressure. As shown in Table 6, an increase in temperature correlates with a reduction in water partial pressure from 2.91 to 1.52 for EBM. The EBM model suggests that a drier reformate promotes more efficient electrochemical reactions, resulting in an overall increase in voltage and LHV efficiency. Furthermore, the rise in hydrogen partial pressure with increasing temperature contributes to improved electrochemical kinetics, augmenting the overall voltage output. The KBM model mirrors these trends to a varying extent, with a decrease of 0.56 in water partial pressure and an increase of 0.49 in hydrogen partial pressure, resulting in a more moderate increase in voltage (ΔV) of from 0.04 V.

Moreover, utilising Equation (4) and the data from Table 6, the average partial pressure ratio between hydrogen and water is observed to increase with a reformer temperature rise from 475 to 725 °C by 300 % for the EBM model and 97 % for the KBM model. As this is a semi-empirical relationship, the increase in ratio translates into a positive voltage change from the reference voltage, indicating an increase in voltage with temperature for both models.

For the impact of reformer pressure, as shown in Fig. 6, the voltages, current density, and LHV efficiency of both the EBM and KBM show better agreement at low pressures, with deviations increasing as the pressure increases. For EBM model, the voltage decreases from 0.74 V to 0.69 V. This trend stems from the effect of pressure on system voltage

(a)



(b)

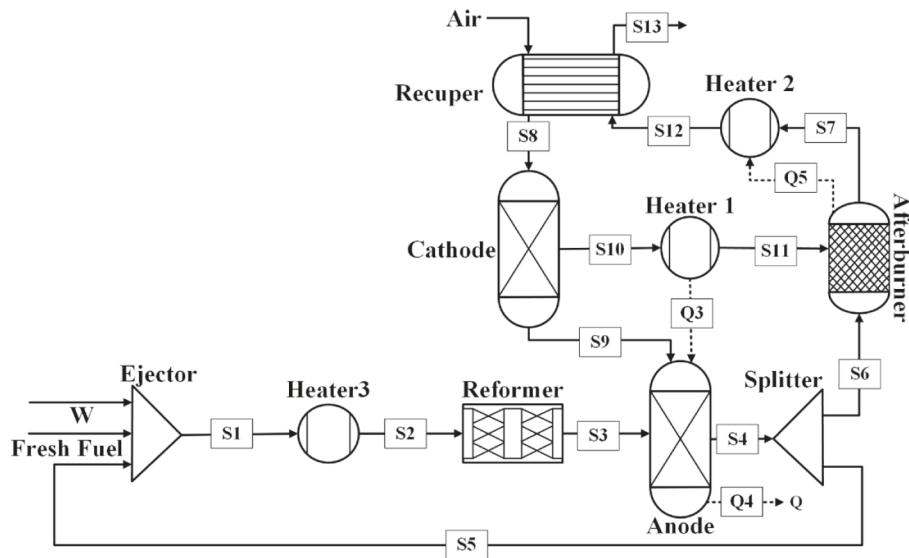


Fig. 2. PFD for a system with an SR reforming subsystem: (a) EBM, (b) KBM flowsheets with reactor and input variations.

output, as described by the Nernst equation. To gain further insight into this, Table 7 presents the partial pressures of relevant species and P_{H_2}/P_{H_2O} at the anode inlet, which decreases from 1.31 to 0.75 for the EBM model, which as expected lead to a reduction in voltage. Simultaneously, the increase in current density from 169 mA/cm² to 180 mA/cm², implies that higher pressure is enhancing mass transport to the electrode surface. The observed decrease in efficiency from 55 % to 52 %, with reference to Equation (6) to (8), a greater amount of hydrogen is required to meet the power demand of the system, thus in turn, increasing the amount of fresh fuel required leading to a reduction in the system LHV efficiency.

Contrastingly, the KBM model demonstrates different outcomes in response to pressure variation. The KBM model indicates an increase in voltage from 0.75 to 0.8 V, aligning more closely with the anticipated impact of pressure on activation polarisation, gas transport, and ohmic losses. This increase in voltage is attributed to the positive influence of higher pressure on electrochemical reactions. As expected, due to

operating at constant power, the KBM model exhibits a decrease in current density from 166 mA/cm² to 157 mA/cm². The observed increase in efficiency from 56 % to 59 % with higher pressure in the KBM model indicates an improvement in overall performance. Table 7 indicates that increasing pressure increases the hydrogen partial pressure and P_{H_2}/P_{H_2O} , suggesting an enriched fuel stream that enhances the reaction at the stack, which increases from 1.53 to 2.97 for the KBM model. Consequently, the voltage and efficiency increase in accordance with the observed changes in partial pressures.

Comparatively, drawing conclusions from Table 7, it is observed that, for the EBM model, the partial pressures of hydrogen and water at the anode increase linearly with increasing reformer pressure at nearly the same rate, being grounded in equilibrium principles. However, there is a slight tilt toward a higher water partial pressure as reformer pressure increases above 15 bar for this simulation, which leads to a decrease in P_{H_2}/P_{H_2O} and a subsequent decline in fuel cell voltage, conflicting with the expected result.

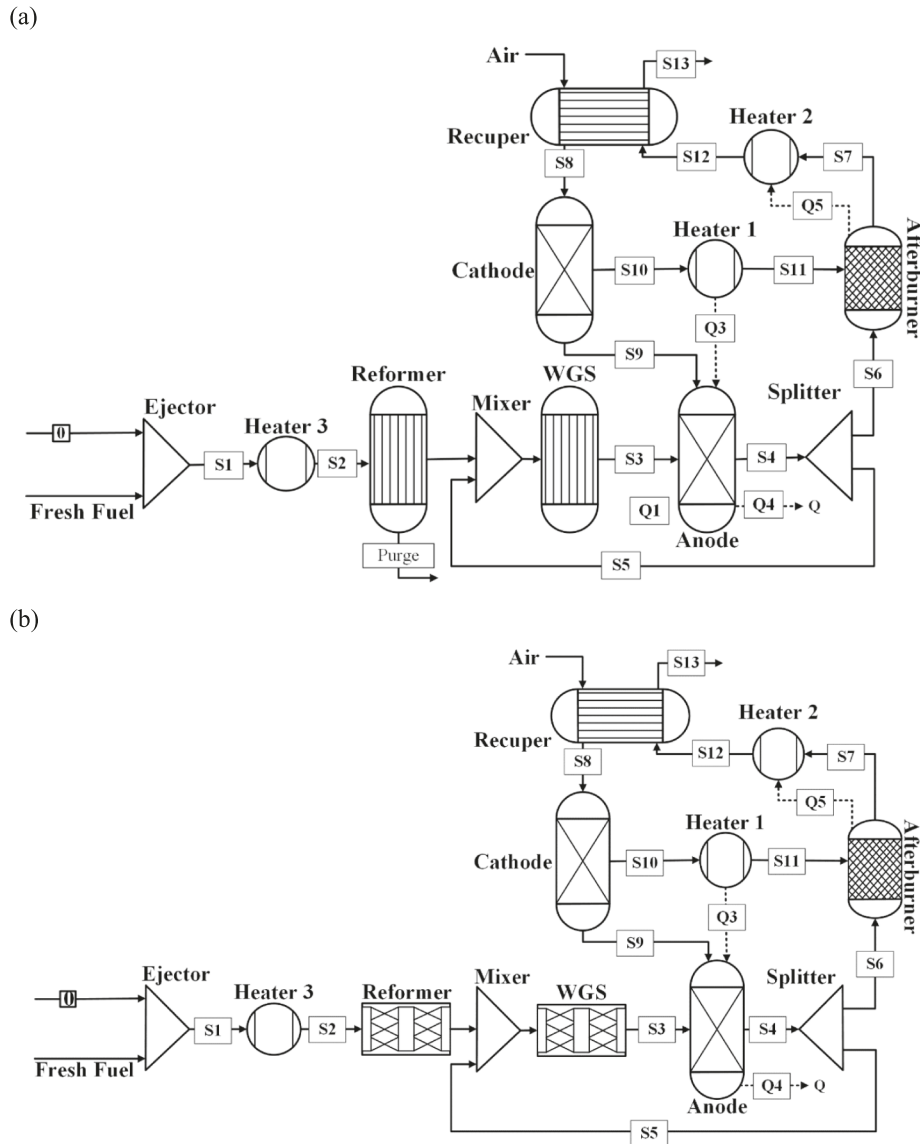


Fig. 3. PFD for a system with a POX reforming subsystem: (a) EBM, and (b) KBM flowsheets with oxygen feed.

In contrast, the KBM model shows that increasing reformer pressure results in hydrogen partial pressure rising at a significantly greater rate than water, thereby increasing P_{H_2}/P_{H_2O} and, correspondingly, the cell voltage (also confirmed from Nernst equation). Hence, the KBM model appears more suitable and accurate than the EBM model for simulating pressurised operation.

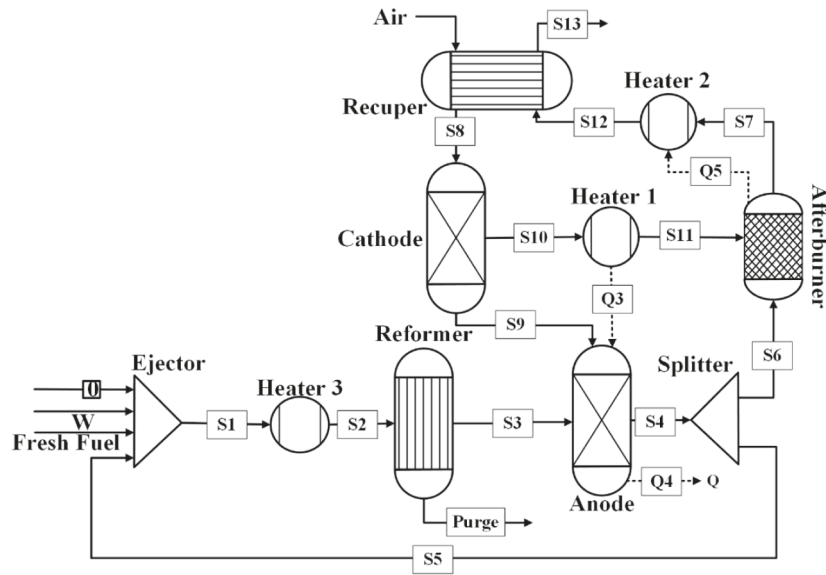
For the impact of steam-to-carbon ratio (S/C) at the reformer inlet on both models, the simulation results in Fig. 7 indicate a decline in SOFC performance with increasing S/C ratios at 5 bar and 475 °C in both the KBM and EBM models, albeit to varying degrees. This observation is somewhat counterintuitive, as one might expect that an increase in the S/C ratio, resulting in a cleaner reformat, would enhance both voltage and efficiency. However, the trends observed suggest otherwise, indicating that diluting the fuel with water leads to a decline in both voltage (as per the Nernst equation) and efficiency. Meanwhile, current density increases, as all other parameters, including fuel flow, remain constant.

For the EBM, the voltage decreases from 0.60 V to 0.56 V as the S/C

ratio increases from 1 to 4.5, with efficiency also declining from 44.60 % to 41.85 %. Similarly, in the KBM, the voltage drops from 0.75 V to 0.63 V, and efficiency decreases from 56.04 % to 47.04 %. Drawing insights from the partial pressure trends in Table 8, the KBM shows a more significant reduction in hydrogen partial pressure, decreasing from 2.22 bar to 1.05 bar, which corresponds to a substantial decline in both voltage and efficiency. In contrast, the EBM, due to its equilibrium-driven nature, shows limited variation, with hydrogen partial pressure decreasing only slightly from 1 to 0.86 across the investigated S/C range. However, this reduction is still enough to lower P_{H_2}/P_{H_2O} , which consequently leads to a decrease in fuel cell voltage and efficiency.

John Bøgild Hansen emphasised [29] that increasing the S/C ratio typically shifts the equilibrium of the water-gas shift (WGS) reaction ($CO + H_2O \leftrightarrow CO_2 + H_2$) towards more CO_2 and H_2 production. However, there is a limit to this benefit, as excess steam can dilute the hydrogen concentration and lower the partial pressure of reactants or affect the thermodynamics of the system by lowering the temperatures

(a)



(b)

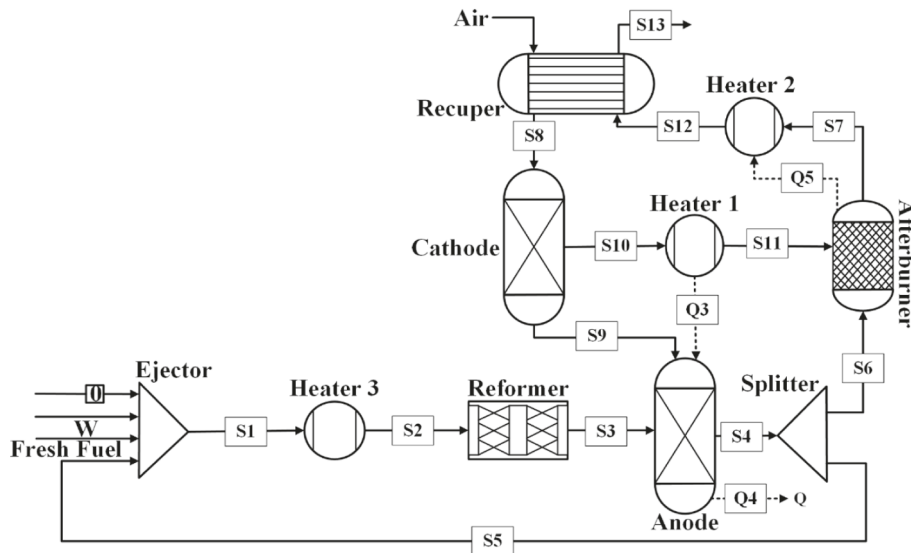


Fig. 4. PFD for a system with an ATR reforming subsystem: (a) EBM, and (b) KBM flowsheet; as above.

in the reformer [30], thereby reducing the reforming reaction rates and leading to lower hydrogen production than expected. This can negatively impact the SOFC voltage and efficiency, consistent with the results observed in the KBM and EBM simulations. Consequently, while EBM can provide a stable baseline, it may not capture the kinetic effects of changing conditions as effectively as KBM. This aligns with the observation that EBM showed less sensitivity to changes in S/C ratio compared to KBM. Hence, the KBM, which accounts for reaction kinetics, may better reflect the real-time kinetics of the reforming process, but it may also be sensitive to the specific kinetic parameters and assumptions used in the simulation.

3.2. Partial oxidation reforming route

Fig. 8 shows the effect of POX process temperature on SOFC performance for both EBM and KBM models. With the KBM, fuel cell voltage

rises exponentially as temperature increases from 500 °C to 750 °C, due to enhanced reaction kinetics and a rapid rise in H_2 partial pressure in the anodic composition. Conversely, the EBM model shows a parabolic voltage increase, reflecting its assumption of instant equilibrium, resulting in gradual changes in reactant and product partial pressures. Table 9 confirms the higher sensitivity of the KBM, as P_{H_2}/P_{H_2O} significantly increases with temperature, while the EBM sees an initial sharp H_2 rise that stabilises at higher temperatures.

The trend observed in EBM indicates efficient initial reforming but limited enhancement at temperatures above 675 °C, as higher temperatures reduce hydrocarbon conversion rates. Due to the exothermic nature of the POX reaction, increased temperature shifts the equilibrium towards reactants, decreasing hydrogen production for anode electrochemical reactions, as shown by the plateau in voltage in Fig. 8. To determine which model better reflects the true behaviour of the POX reaction across increasing temperatures, a comparison of the trends

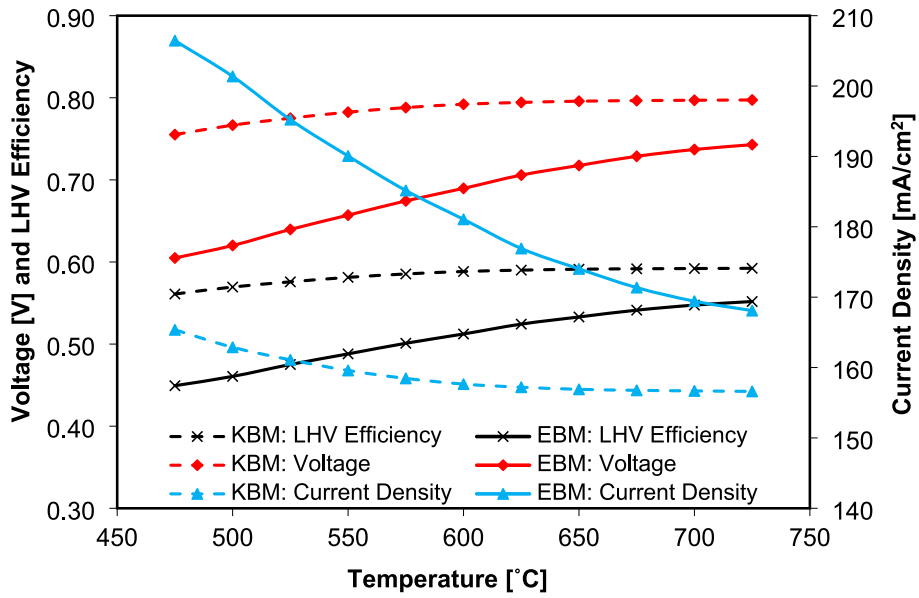


Fig. 5. Effect of SR-based reformer temperature on SOFC performance, predicted by EBM and KBM.

Table 6

Species partial pressure (bar) vs temperature at 5 bar.

SR Model	Component	Temperature [°C]											
		475	500	525	550	575	600	625	650	675	700	725	
EBM	H ₂ O	2.91	2.72	2.54	2.36	2.19	2.03	1.88	1.76	1.65	1.57	1.52	
	H ₂	1.00	1.14	1.29	1.43	1.57	1.70	1.81	1.91	2.00	2.06	2.10	
	CO	0.03	0.06	0.09	0.12	0.17	0.23	0.30	0.38	0.45	0.51	0.57	
	CO ₂	0.64	0.69	0.73	0.75	0.76	0.76	0.74	0.71	0.68	0.64	0.6	
	N ₂	0.42	0.39	0.36	0.33	0.31	0.28	0.26	0.24	0.23	0.22	0.21	
	P _{H₂} /P _{H₂O}	0.34	0.42	0.51	0.61	0.72	0.84	0.97	1.09	1.21	1.31	1.38	
KBM	H ₂ O	1.45	1.29	1.17	1.08	1.01	0.96	0.93	0.91	0.9	0.9	0.89	
	H ₂	2.22	2.36	2.46	2.54	2.61	2.65	2.67	2.69	2.7	2.70	2.71	
	CO	0.02	0.03	0.03	0.03	0.03	0.03	0.03	0.03	0.03	0.03	0.03	
	CO ₂	1.06	1.09	1.12	1.14	1.16	1.17	1.17	1.18	1.18	1.18	1.18	
	N ₂	0.25	0.23	0.22	0.21	0.20	0.20	0.20	0.19	0.19	0.19	0.19	
	P _{H₂} /P _{H₂O}	1.53	1.83	2.10	2.36	2.59	2.76	2.88	2.95	3.00	3.02	3.03	

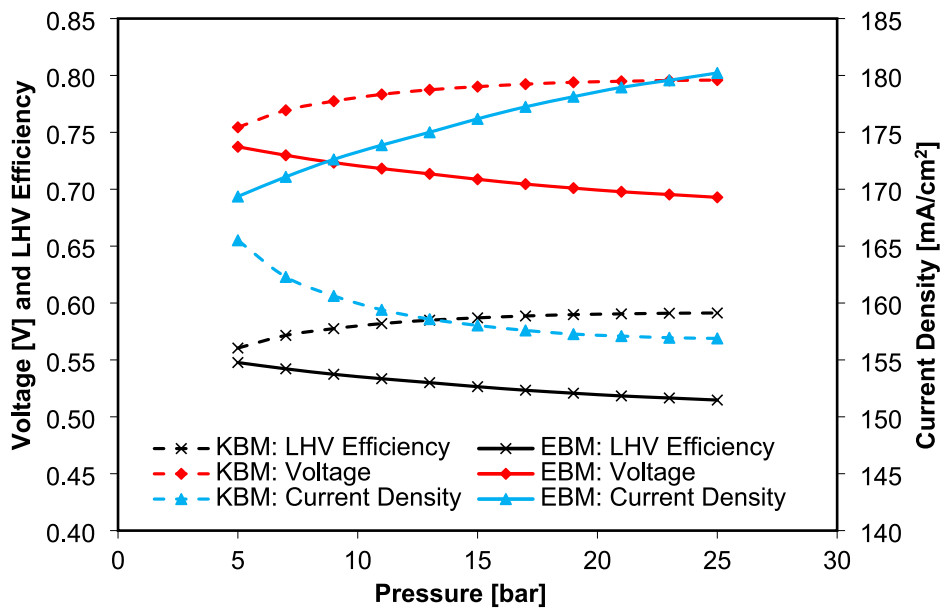


Fig. 6. Effect of SR-based reformer pressure on SOFC performance, predicted by EBM and KBM.

Table 7
Reformer outlet partial pressures at varying SR pressures.

SR Model	Component	Pressure [bar]										
		5	7	9	11	13	15	17	19	21	23	25
EBM	H ₂ O	1.57	2.33	3.14	3.98	4.87	5.78	6.72	7.68	8.65	9.64	10.7
	H ₂	2.06	2.78	3.45	4.10	4.71	5.30	5.87	6.43	6.97	7.50	8.02
	CO	0.51	0.67	0.80	0.92	1.03	1.13	1.22	1.31	1.39	1.46	1.54
	CO ₂	0.64	0.91	1.18	1.46	1.73	2.00	2.28	2.54	2.81	3.08	3.34
	N ₂	0.22	0.32	0.43	0.54	0.66	0.79	0.92	1.05	1.18	1.32	1.46
KBM	P _{H₂} /P _{H₂O}	1.31	1.19	1.10	1.03	0.97	0.92	0.87	0.84	0.81	0.78	0.75
	H ₂ O	1.45	1.76	2.05	2.34	2.63	2.93	3.24	3.55	3.87	4.19	4.53
	H ₂	2.22	3.35	4.48	5.62	6.76	7.90	9.02	10.2	11.3	12.4	13.5
	CO	0.02	0.04	0.05	0.06	0.07	0.09	0.10	0.11	0.12	0.13	0.15
	CO ₂	1.06	1.54	2.03	2.52	3.00	3.49	3.97	4.45	4.93	5.41	5.88
	N ₂	0.25	0.32	0.39	0.46	0.53	0.60	0.67	0.75	0.82	0.89	0.97
	P _{H₂} /P _{H₂O}	1.53	1.90	2.19	2.40	2.57	2.70	2.78	2.86	2.91	2.95	2.97

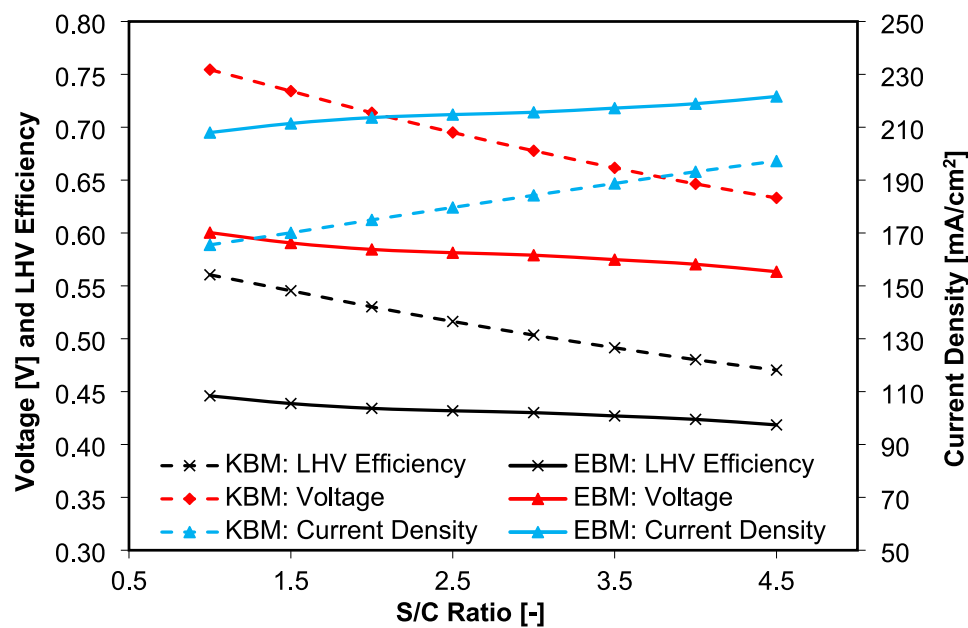


Fig. 7. Effect of fuel feed S/C ratio in an SR-based reformer on SOFC system performance predicted by the EBM and KBM models.

Table 8
Components partial pressure (bar) variations with steam-to-carbon ratio.

SR Model	Component	S/C Ratio								
		1	1.5	2	2.5	3	3.5	4	4.5	
EBM	H ₂ O	2.90	3.14	3.30	3.42	3.51	3.57	3.63	3.68	
	H ₂	1.00	0.98	0.96	0.94	0.92	0.90	0.89	0.86	
	CO	0.04	0.03	0.02	0.01	0.01	0.01	0.01	0.01	
	CO ₂	0.64	0.53	0.46	0.41	0.37	0.35	0.33	0.31	
	N ₂	0.42	0.32	0.26	0.21	0.19	0.17	0.15	0.13	
KBM	P _{H₂} /P _{H₂O}	0.34	0.31	0.29	0.28	0.26	0.25	0.24	0.23	
	H ₂ O	1.46	1.84	2.20	2.52	2.81	3.05	3.27	3.46	
	H ₂	2.22	2.04	1.84	1.64	1.47	1.31	1.17	1.05	
	CO	0.02	0.02	0.02	0.02	0.02	0.01	0.01	0.01	
	CO ₂	1.05	0.89	0.74	0.64	0.54	0.47	0.40	0.35	
	N ₂	0.25	0.22	0.20	0.18	0.16	0.15	0.14	0.13	
	P _{H₂} /P _{H₂O}	1.53	1.11	0.84	0.65	0.52	0.43	0.36	0.30	

observed in the reformer results was performed against several experimental data found in the literature. It was found that at a pressure of 5 bar and above with a catalyst, the methane conversion curve follows the trend observed in the KBM [31,32]. At atmospheric pressure without a catalyst or at very low catalyst loading, the methane conversion curve also follows the trend observed in the KBM [33]. Conversely, at atmospheric pressure with a catalyst, the methane conversion curve follows

the trend observed in the EBM [32–35].

The observed trends indicate that the presence of a catalyst and the operating pressure significantly influence whether the reaction is kinetically, or equilibrium limited. This behaviour stems from the fact that at higher pressures, reaction kinetics are often the limiting factor (i.e., kinetic dominance). The presence of a catalyst enhances the reaction rate by providing active sites, leading to higher conversion rates that

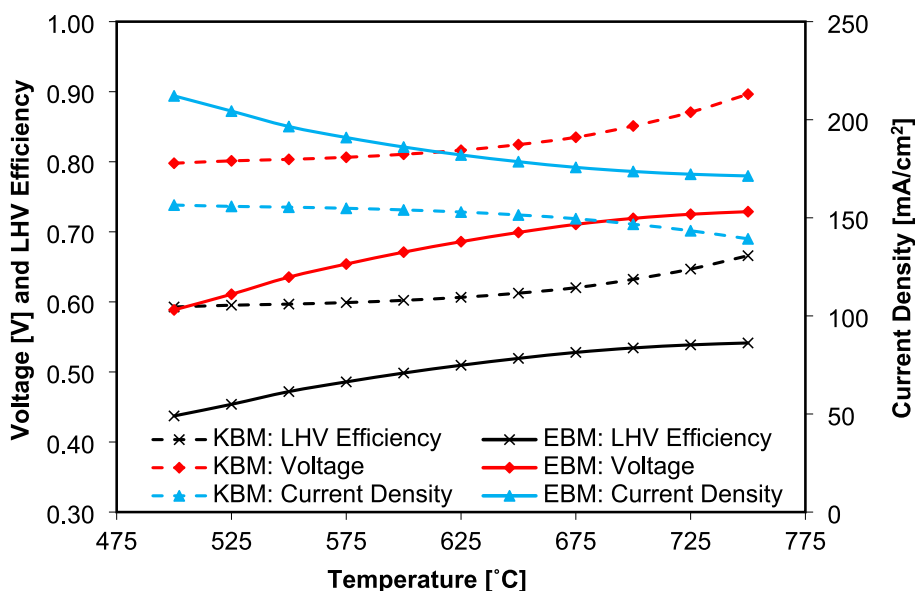


Fig. 8. Effect of temperature on a POX-based reformer on SOFC system performance predicted by KBM and EBM.

Table 9

Reformer inlet/outlet partial pressures by KBM and EBM vs temperatures.

POX Model	Component	Temperature [°C]											
		500	525	550	575	600	625	650	675	700	725	750	
EBM	CO	0.32	0.29	0.26	0.22	0.19	0.16	0.13	0.10	0.06	0.03	0.00	
	H ₂ O	0.25	0.33	0.40	0.47	0.54	0.62	0.69	0.76	0.84	0.91	0.98	
	H ₂	0.16	0.29	0.41	0.54	0.66	0.79	0.92	1.04	1.17	1.29	1.42	
	CO ₂	0.00	0.13	0.25	0.38	0.50	0.63	0.76	0.88	1.01	1.13	1.26	
	CH ₄	2.97	2.74	2.50	2.27	2.03	1.80	1.56	1.33	1.09	0.86	0.62	
	C ₂ H ₆	0.00	0.00	0.00	0.00	0.00	0.00	0.00	0.00	0.00	0.00	0.00	
	C ₃ H ₈	0.00	0.00	0.00	0.00	0.00	0.00	0.00	0.00	0.00	0.00	0.00	
	O ₂	0.77	0.74	0.70	0.67	0.63	0.60	0.56	0.53	0.49	0.46	0.42	
	N ₂	0.52	0.50	0.48	0.45	0.43	0.41	0.39	0.37	0.34	0.32	0.30	
	P _{H₂} /P _{H₂O}	0.64	0.88	1.04	1.14	1.22	1.28	1.33	1.37	1.40	1.42	1.45	
KBM	CO	0.00	0.00	0.00	0.00	0.00	0.00	0.00	0.00	0.00	0.00		
	H ₂ O	0.68	0.66	0.66	0.64	0.62	0.60	0.57	0.53	0.46	0.39	0.31	
	H ₂	1.63	1.66	1.68	1.70	1.74	1.78	1.85	1.94	2.06	2.20	2.37	
	CO ₂	1.22	1.22	1.23	1.24	1.24	1.26	1.27	1.29	1.32	1.36	1.40	
	CH ₄	0.76	0.75	0.75	0.74	0.72	0.70	0.66	0.62	0.57	0.50	0.42	
	C ₂ H ₆	0.01	0.00	0.00	0.00	0.00	0.00	0.00	0.00	0.00	0.00	0.00	
	C ₃ H ₈	0.00	0.00	0.00	0.00	0.00	0.00	0.00	0.00	0.00	0.00	0.00	
	O ₂	0.39	0.38	0.38	0.37	0.36	0.35	0.34	0.32	0.29	0.25	0.21	
	N ₂	0.32	0.32	0.31	0.31	0.31	0.31	0.31	0.31	0.30	0.30	0.29	
	P _{H₂} /P _{H₂O}	2.40	2.50	2.56	2.65	2.78	2.97	3.26	3.69	4.45	5.61	7.61	

align with the KBM, which focuses on reaction kinetics. In the absence of a catalyst, there are no surface-mediated reactions to alter the conversion dynamics, so the reaction relies solely on the inherent kinetic energy of the reactants provided by the reaction temperature. At atmospheric pressure, the reaction progresses according to the kinetic parameters intrinsic to hydrocarbon and oxygen interactions at the specified temperature, which aligns with KBM predictions. Meanwhile, at atmospheric pressure, the presence of a catalyst facilitates surface reactions that rapidly drive the system towards equilibrium (i.e., equilibrium control). The catalyst lowers activation energies and promotes the attainment of equilibrium conditions more rapidly, which aligns with EBM predictions.

Therefore, it can be mentioned that at high pressures with a catalyst,

the POX reaction is kinetically controlled, making the KBM more accurate for predicting hydrocarbon conversion and product distributions. The KBM is also preferable at atmospheric pressure without a catalyst or with minimal catalyst loading, where reaction dynamics remain kinetically limited. Conversely, at atmospheric pressure with a catalyst, equilibrium conditions dominate, favouring the EBM for accurate hydrocarbon conversion and product distribution predictions.

The observed results using KBM, as shown in Fig. 9, conducted at 700 °C with a S/C ratio of 0.9 and an O/C ratio of 0.5, indicate that as the pressure increases from 1 to 10 bar, the fuel cell voltage, current density, and LHV efficiency progressively improve.

This trend is attributed to the fact that increased pressure enhances the reaction kinetics, leading to more effective reforming of hydrocar-

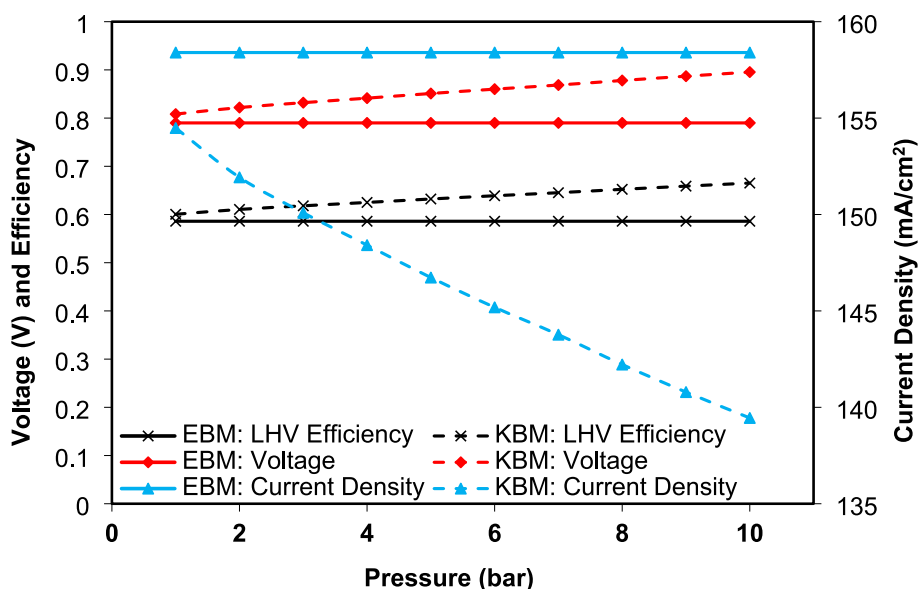


Fig. 9. Effect of pressure on a POX-based reformer on SOFC system performance predicted by KBM and EBM.

Table 10
Reformer inlet/outlet partial pressure by KBM and EBM vs pressures.

POX Model	Component	Pressure [bar]									
		1	2	3	4	5	6	7	8	9	10
EBM	CO	0.05	0.09	0.14	0.18	0.23	0.27	0.32	0.36	0.41	0.45
	H ₂ O	0.36	0.71	1.07	1.42	1.78	2.13	2.49	2.85	3.20	3.56
	H ₂	0.32	0.64	0.95	1.27	1.59	1.91	2.23	2.55	2.87	3.19
	CO ₂	0.18	0.36	0.54	0.72	0.91	1.09	1.27	1.45	1.64	1.82
	CH ₄	0.00	0.00	0.00	0.00	0.00	0.00	0.00	0.00	0.00	0.00
	C ₂ H ₆	0.00	0.00	0.00	0.00	0.00	0.00	0.00	0.00	0.00	0.00
	C ₃ H ₈	0.00	0.00	0.00	0.00	0.00	0.00	0.00	0.00	0.00	0.00
	O ₂	0.06	0.12	0.18	0.25	0.31	0.37	0.43	0.49	0.56	0.62
	N ₂	0.04	0.08	0.11	0.15	0.18	0.22	0.25	0.29	0.32	0.36
	P _{H₂} /P _{H₂O}	0.89	0.89	0.89	0.89	0.90	0.90	0.90	0.90	0.90	0.90
	KBM	CO	0.01	0.00	0.00	0.00	0.00	0.00	0.00	0.00	0.00
H ₂ O		0.13	0.23	0.32	0.40	0.46	0.52	0.56	0.59	0.61	0.63
H ₂		0.34	0.73	1.15	1.59	2.06	2.55	3.06	3.60	4.16	4.72
CO ₂		0.24	0.51	0.77	1.04	1.32	1.61	1.90	2.19	2.49	2.80
CH ₄		0.14	0.27	0.38	0.48	0.57	0.64	0.71	0.76	0.80	0.84
C ₂ H ₆		0.00	0.00	0.00	0.00	0.00	0.00	0.00	0.00	0.00	0.00
C ₃ H ₈		0.00	0.00	0.00	0.00	0.00	0.00	0.00	0.00	0.00	0.00
O ₂		0.07	0.14	0.19	0.24	0.29	0.33	0.36	0.39	0.41	0.43
N ₂		0.06	0.12	0.18	0.24	0.30	0.36	0.41	0.47	0.52	0.58
P _{H₂} /P _{H₂O}		2.70	3.17	3.56	3.97	4.45	4.95	5.47	6.11	6.79	7.52

bons and greater hydrogen production. The increase in the P_{H_2}/P_{H_2O} (as seen in Table 10) directly improves the electrochemical reactions in the SOFC, leading to higher voltage and efficiency. This improvement originates from an increased anodic voltage change (Equation (4)) and a decreasing current density (as shown in Fig. 9). The linear increase in voltage with KBM reflects enhanced reaction rates at higher pressures, which is typical in kinetic-dominated processes.

In contrast, the EBM-based simulations show that pressure changes in the reformer have no significant impact on the SOFC performance indicators, with the voltage, current density, and LHV efficiency remaining constant across all pressures, as shown in Fig. 9. This observation is rooted in the fact that EBM assumes the system rapidly reaches equilibrium, regardless of pressure. Since the reactions are assumed to

be at equilibrium instantly, increasing pressure does not significantly affect the equilibrium compositions, as shown in the unchanging P_{H_2}/P_{H_2O} ratio across pressures from 1 bar to 10 bar in Table 10, leading to constant SOFC performance.

Consequently, it is preferred to use KBM for POX-based reformers operating at higher pressures, as this model more accurately reflects the improvements in SOFC performance due to enhanced reaction kinetics. On the other hand, EBM should be employed for simplified or rapid assessments where quick, equilibrium-based evaluations are preferred, and pressure is not a critical variable. However, EBM should be applied cautiously when pressure changes are expected to significantly influence reaction dynamics.

The investigation of the effect of the O/C ratio on a POX-based

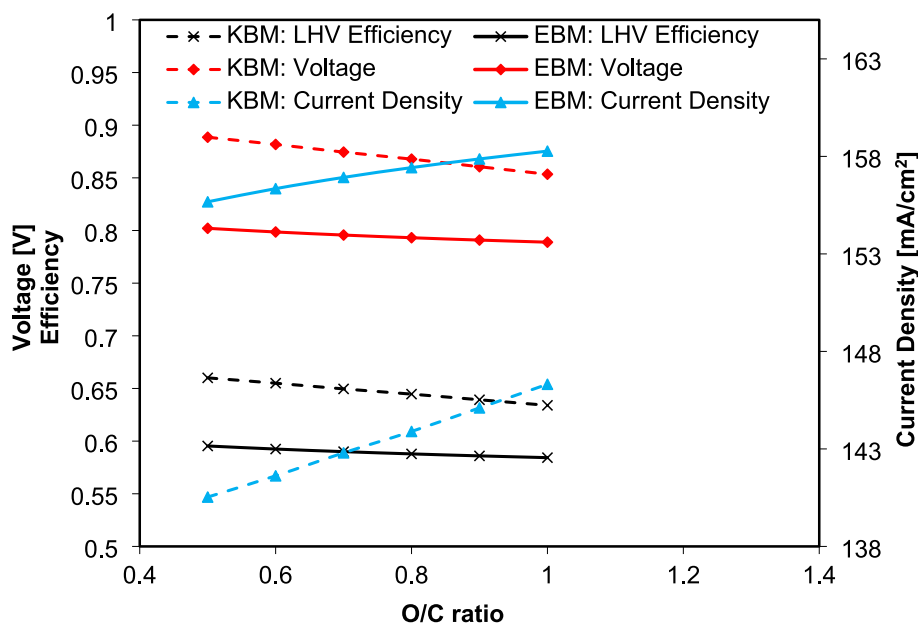


Fig. 10. Effect of O/C ratio of a POX-based reformer on SOFC system performance predicted by KBM and EBM.

Table 11
Reformer inlet/outlet partial pressures by KBM and EBM vs O/C ratios.

PoX Model	Component	O/C Ratio					
		0.50	0.60	0.70	0.80	0.90	1.00
EBM	CO	0.05	0.05	0.05	0.05	0.05	0.05
	H ₂ O	0.35	0.35	0.35	0.35	0.35	0.35
	H ₂	0.37	0.36	0.35	0.33	0.32	0.31
	CO ₂	0.19	0.19	0.19	0.18	0.18	0.18
	CH ₄	0.00	0.00	0.00	0.00	0.00	0.00
	C ₂ H ₆	0.00	0.00	0.00	0.00	0.00	0.00
	C ₃ H ₈	0.00	0.00	0.00	0.00	0.00	0.00
	O ₂	0.00	0.02	0.03	0.05	0.06	0.08
	N ₂	0.04	0.04	0.04	0.04	0.04	0.04
	P _{H₂} /P _{H₂O}	1.06	1.03	1.00	0.94	0.91	0.89
KBM	CO	0.02	0.02	0.02	0.02	0.02	0.02
	H ₂ O	0.07	0.07	0.07	0.08	0.08	0.08
	H ₂	0.47	0.45	0.43	0.42	0.39	0.38
	CO ₂	0.26	0.25	0.25	0.24	0.23	0.22
	CH ₄	0.08	0.08	0.09	0.09	0.09	0.10
	C ₂ H ₆	0.00	0.00	0.00	0.00	0.00	0.00
	C ₃ H ₈	0.00	0.00	0.00	0.00	0.00	0.00
	O ₂	0.04	0.06	0.08	0.11	0.13	0.16
	N ₂	0.06	0.06	0.06	0.06	0.05	0.05
	P _{H₂} /P _{H₂O}	6.92	6.39	5.86	5.42	4.97	4.57

reformer at 900 °C, with a S/C ratio of 0.9 and a pressure of 1 bar, as presented in Fig. 10, reveals that as the O/C ratio increases from 0.5 to 1.0 for KBM, the SOFC voltage and LHV efficiency gradually decrease. This decline in voltage and efficiency can be attributed to the changing composition of the reformate gases. With higher O/C ratios, more oxygen is available, leading to more complete oxidation reactions. This results in lower hydrogen production and an increased presence of steam in the reformate, as seen in the reformer outlet partial pressures (Table 11).

Consequently, the decrease in P_{H₂}/P_{H₂O} from 6.9 to 4.6 reduces voltage and efficiency in SOFC anode reactions. While the EBM model also shows declining voltage and efficiency with increasing O/C ratio (Fig. 10), changes are minimal, with voltage consistently around 0.80 V,

reflecting the EBM's equilibrium assumption and limited sensitivity to reformate composition. Hydrogen production decreases slightly, along with the P_{H₂}/P_{H₂O} ratio (Table 11), resulting in consistent but lower performance than the KBM.

3.3. Autothermal reforming route (ATR)

The autothermal model combines steam reforming and partial oxidation, enhancing heat and temperature management over other models [36]. Key operating variables include temperature, pressure, S/C ratio, and O/C ratio.

As shown in Fig. 11, the SOFC voltage increases progressively from 0.718 V at 620 °C to 0.832 V at 1000 °C in the KBM as well as the efficiency. This behaviour can be attributed to enhanced reaction kinetics at higher temperatures, which promote more efficient hydrocarbon reforming, resulting in higher hydrogen production. The rise in the P_{H₂}/P_{H₂O} in the KBM, as shown in Table 12, facilitates higher cell voltages and improved efficiency.

Table 13 shows increasing CH₄ conversion with increasing temperature, supporting the kinetic dominance predicted by the KBM and its accurate capture of enhanced reaction kinetics at higher temperatures. In contrast, Fig. 11 shows that, for EBM, the cell voltage remains stable between 0.759 V and 0.748 V from 620 °C to 1000 °C, indicating its lower sensitivity to temperature.

This behaviour is expected, as the EBM assumes near-instant equilibrium, resulting in limited temperature sensitivity. Although Table 13 shows higher CH₄ conversion for the EBM than the KBM, at lower temperatures, hydrogen production increases less effectively at higher temperatures, suggesting that the EBM high CH₄ conversion does not accurately capture hydrogen production kinetics, thereby reducing cell's performance.

The KBM CH₄ conversion trends align with experimental findings, where temperature critically influences CH₄ reforming kinetics. For example, Karakaya et al. [37] observed significant increases in CH₄ conversion and CO selectivity with temperature, highlighting kinetic dominance. Similarly, Ayabe et al. [38] found that 10 wt% Ni/Al₂O₃ catalysed CH₄ reforming matched KBM predictions during heating,

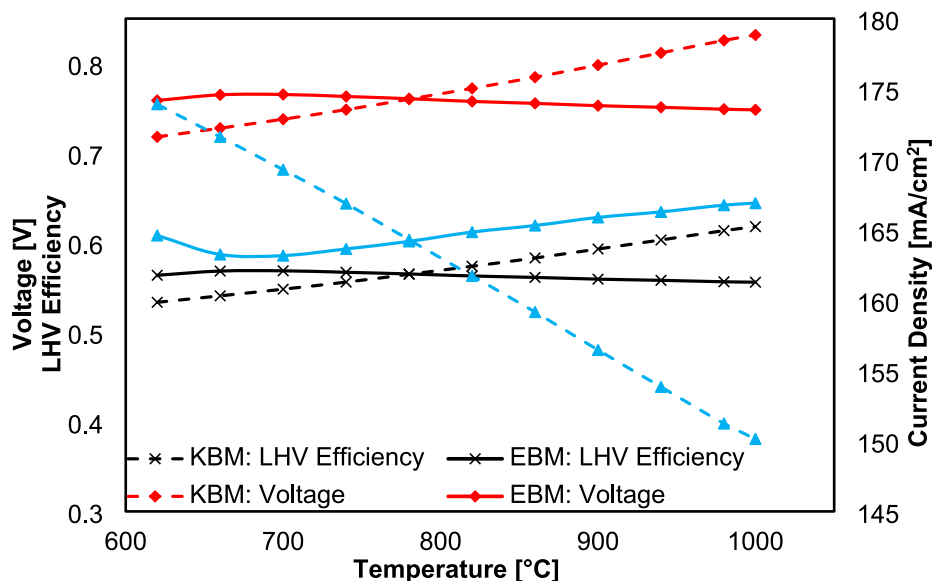


Fig. 11. Effect of temperature of an autothermal-based reformer on SOFC performance, predicted by KBM and EBM at 1 bar, 0.5O/C and S/C of 0.9.

Table 12

Reformer outlet partial pressures by KBM and EBM vs temperatures and pressures.

ATR Model	Component	Temperature [°C]			Pressure [bar]		
		620	820	1000	1	5	10
EBM	CO	0.09	0.15	0.17	0.09	0.25	0.36
	H ₂ O	0.28	0.28	0.30	0.28	1.80	4.02
	H ₂	0.43	0.43	0.41	0.43	1.51	2.43
	CO ₂	0.14	0.10	0.08	0.14	0.73	1.45
	CH ₄	0.02	0.00	0.00	0.02	0.46	1.25
	C ₂ H ₆	0.00	0.00	0.00	0.00	0.00	0.00
	C ₃ H ₈	0.00	0.00	0.00	0.00	0.00	0.00
	O ₂	0.00	0.00	0.00	0.00	0.00	0.00
	N ₂	0.04	0.04	0.04	0.04	0.23	0.49
	P _{H₂} /P _{H₂O}	1.53	1.51	1.36	1.54	0.84	0.60
KBM	CO	0.00	0.00	0.00	0.01	0.01	0.01
	H ₂ O	0.23	0.18	0.12	0.25	0.73	0.71
	H ₂	0.25	0.33	0.43	0.23	1.95	5.07
	CO ₂	0.10	0.12	0.15	0.09	0.68	1.70
	CH ₄	0.21	0.17	0.12	0.22	0.72	0.85
	C ₂ H ₆	0.00	0.00	0.00	0.00	0.00	0.00
	C ₃ H ₈	0.00	0.00	0.00	0.00	0.00	0.00
	O ₂	0.15	0.14	0.13	0.16	0.69	1.26
	N ₂	0.05	0.05	0.04	0.05	0.22	0.41
	P _{H₂} /P _{H₂O}	1.08	1.79	3.55	0.94	2.68	7.19

Table 13

CH₄ conversion and H₂ output vs. reformer temperature by EBM and KBM.

ATR Model	KBM		EBM		
	Temperature (°C)	CH ₄ (%)	H ₂ (%)	CH ₄ (%)	H ₂ (%)
620	6.17	–	87.59	–	
660	8.26	7.81	95.07	6.95	
700	10.75	7.84	98.27	1.83	
740	13.62	8.15	99.40	–0.37	
780	16.84	8.61	99.78	–0.89	
820	20.38	8.52	98.66	–1.28	
860	24.18	8.38	99.97	–0.94	
900	28.23	8.43	99.98	–1.18	
940	32.42	7.96	99.99	–0.82	
980	36.72	7.54	100.0	–1.01	
1000	38.82	3.20	100.0	–0.30	

while cooling followed equilibrium, consistent with EBM data obtained in this study. Arguably, the EBM data may be less representative of real-world behaviour due to its assumption of ideal equilibrium conditions rarely achieved in practice. Thus, the KBM is recommended for accurate SOFC performance prediction at high temperatures, whereas the EBM is suitable for quick assessments or equilibrium-dominant conditions.

The study also examines the impact of pressure on ATR and SOFC performance using the KBM and EBM models at 620 °C, with an S/C ratio of 0.9 and O/C ratio of 0.5 (Fig. 12). The KBM model predicts that as pressure increases from 1 to 10 bar, SOFC efficiency increases from 0.54 to 0.70, voltage from 0.73 V to 0.94 V, and current density decreases from 172.0 to 133.2 mA/cm², indicating that higher pressures lead to an increase in P_{H₂}/P_{H₂O} (Table 12), consistent with the thermodynamic principle favouring higher hydrogen partial pressure at the anode.

Conversely, the EBM model shows efficiency decreasing from 0.56 to 0.50 and voltage from 0.76 V to 0.67 V with increasing pressure, aligning with findings that high methane partial pressure can inhibit reforming reactions and reduce hydrogen yield, as supported by literature on methane retention and incomplete reforming at high pressures [39–41].

Fig. 13 shows that SOFC performance declines with increasing S/C ratios (0.5 to 1.5) at 620 °C, 1 bar, and an O/C of 0.5 for both KBM and EBM models, with a negative correlation in voltage and LHV efficiency due to the WGS reaction.

Higher S/C ratios push WGS equilibrium towards CO₂ and H₂ production, increasing water partial pressure, diluting hydrogen, and reducing P_{H₂}/P_{H₂O} (Table 14), which lowers the cell voltage as described by Equation (1) to (8) [37]. This effect is more pronounced in the KBM, with sharper voltage drops from 0.837 V to 0.672 V, while EBM shows a smaller decline (0.802 V to 0.754 V). Consequently, KBM kinetic sensitivity offers a detailed view of SOFC response under variable S/C reformer conditions, making it ideal for applications with variable feeds, while the stability of EBM favours scenarios with steady feeds.

Fig. 14 shows that increasing the O/C ratio decreases SOFC voltage and LHV efficiency in the KBM due to higher oxidation, which reduces hydrogen and CO while increasing water and CO₂ production. As the O/C ratio increases from 0.5 to 1.0, hydrogen partial pressure drops (0.29 bar to 0.17 bar), and P_{H₂}/P_{H₂O} declines from 2.93 to 1.16 (Table 14). The EBM, however, shows stable voltage and efficiency, reflecting its equilibrium-based assumptions that ignore kinetic variations in hydrogen production. Experimental studies by Karakaya et al. [37] and

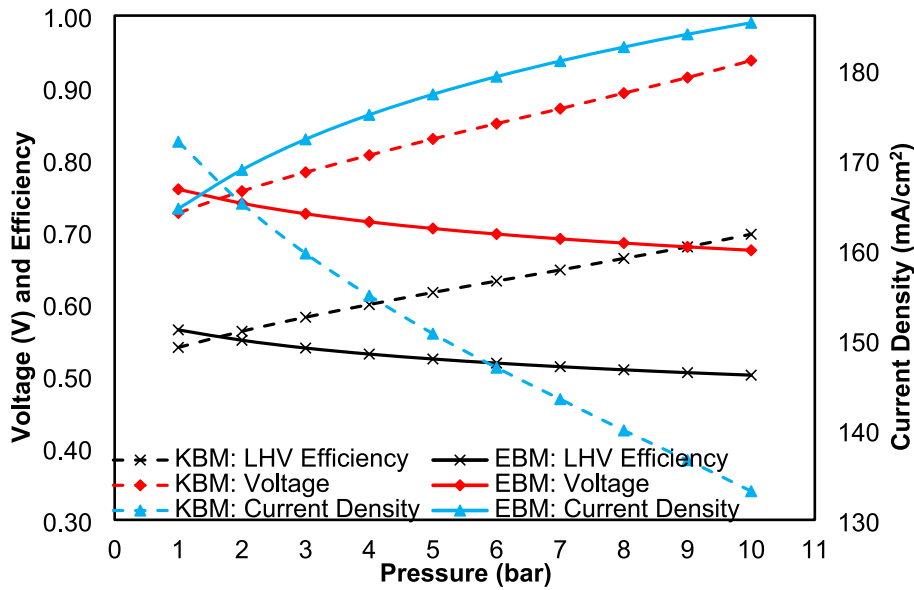


Fig. 12. Effect of pressure on an autothermal-based reformer on SOFC performance, predicted by KBM and EBM (at $T = 620\text{ }^{\circ}\text{C}$, $O/C = 0.5$ and $S/C = 0.9$).

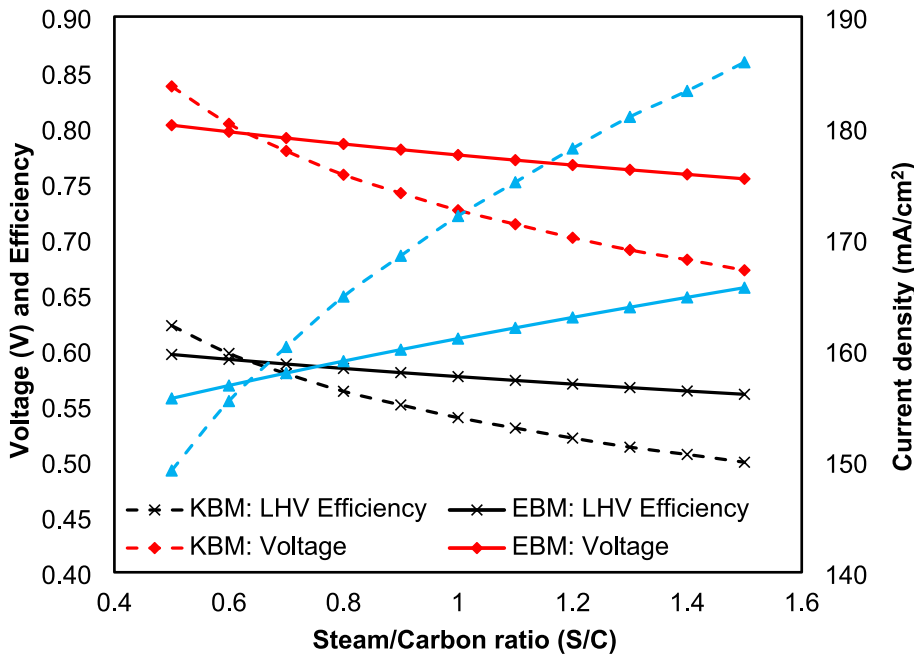


Fig. 13. Effect of S/C on an autothermal-based reformer on SOFC performance, predicted by KBM and EBM (at $T = 620\text{ }^{\circ}\text{C}$, $O/C = 0.5$ and $P = 1\text{ bar}$).

Matheus et al. [41] support KBM accuracy, making it suitable for dynamic systems, while EBM is useful for equilibrium-dominant cases.

4. Conclusion

This study provides a detailed comparison of EBM and KBM in simulating SOFC performance integrated with different reforming routes including SR, POX, and ATR within the BoP system. The objective was to evaluate the accuracy and reliability of each model in predicting system-level effects on SOFC performance across varying operating conditions, including temperature, pressure, S/C, and O/C ratios.

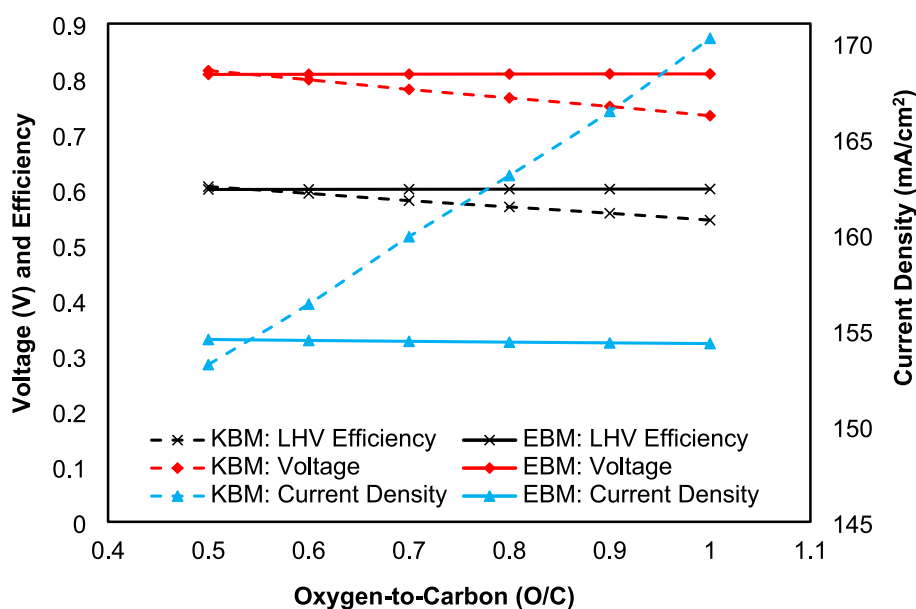
The results show that KBM provides a more detailed representation

of SOFC varying behaviour, especially in kinetically driven scenarios. For example, in the SR route, KBM displayed a sharper voltage increase with temperature than EBM, which showed a smoother response. Similarly, in the POX route, KBM effectively captured the exponential voltage rise with temperature, unlike a more gradual, linear-parabolic trend observed for EBM. While EBM offers a quick assessment of thermodynamic equilibrium, it has limitations under varying pressure and feed conditions due to its instant equilibrium assumption, impacting accuracy in kinetically influenced conditions. The distinct differences between the models highlight their suitability for different scenarios: EBM is ideal for conditions favouring equilibrium, such as atmospheric pressure with catalysts that quickly reach equilibrium, while KBM is

Table 14

Reformer outlet partial pressures by KBM and EBM vs S/C and O/C ratios.

ATR Model	Component	S/C ratio			O/C ratio		
		0.5	1	1.5	0.5	0.7	1
EBM	CO	0.13	0.10	0.08	0.25	0.24	0.23
	H ₂ O	0.18	0.24	0.30	0.10	0.10	0.09
	H ₂	0.46	0.45	0.44	0.29	0.28	0.26
	CO ₂	0.12	0.13	0.13	0.11	0.11	0.10
	CH ₄	0.06	0.04	0.02	0.00	0.00	0.00
	C ₂ H ₆	0.00	0.00	0.00	0.00	0.00	0.00
	C ₃ H ₈	0.00	0.00	0.00	0.01	0.01	0.01
	O ₂	0.00	0.00	0.00	0.18	0.21	0.25
	N ₂	0.05	0.04	0.04	0.06	0.06	0.05
	P _{H₂} /P _{H₂O}	2.52	1.86	1.46	2.90	2.90	2.89
KBM	CO	0.01	0.00	0.00	0.01	0.01	0.01
	H ₂ O	0.09	0.24	0.35	0.10	0.12	0.14
	H ₂	0.32	0.26	0.21	0.29	0.24	0.17
	CO ₂	0.12	0.10	0.08	0.11	0.10	0.12
	CH ₄	0.25	0.22	0.20	0.25	0.24	0.21
	C ₂ H ₆	0.00	0.00	0.00	0.00	0.00	0.00
	C ₃ H ₈	0.00	0.00	0.00	0.00	0.00	0.00
	O ₂	0.15	0.13	0.11	0.18	0.00	0.30
	N ₂	0.06	0.05	0.05	0.06	0.05	0.05
	P _{H₂} /P _{H₂O}	3.78	1.06	0.59	2.93	1.98	1.16

Fig. 14. Effect of O/C on an autothermal-based reformer on SOFC performance, predicted by KBM and EBM (at $T = 620$ °C, $S/C = 0.5$ and $P = 1$ bar).

preferable in systems where reaction kinetics and mass transport limitations are critical, such as high-pressure operations or without catalysts.

Given these findings, KBM is the preferred model for accurately predicting SOFC performance with SR, POX, and ATR reforming routes, especially in varying operating conditions. While EBM is useful for initial assessments, it should be applied cautiously in scenarios where kinetic effects are significant.

CRedit authorship contribution statement

Clyde-Theodore N. Batista: Writing – review & editing, Writing – original draft, Visualization, Validation, Software, Methodology, Investigation, Formal analysis, Conceptualization. **Kazeem Ayodeji Mohammed:** Writing – review & editing, Writing – original draft, Visualization, Validation, Software, Methodology, Investigation, Formal analysis, Conceptualization. **Amirpiran Amiri:** Writing – review & editing, Supervision, Software, Methodology, Funding acquisition,

Formal analysis, Conceptualization. **Neda Azimi:** Writing – original draft, Software, Methodology, Investigation, Formal analysis, Conceptualization. **Robert Steinberger-Wilckens:** Writing – review & editing, Validation, Supervision, Formal analysis, Conceptualization.

Declaration of competing interest

The authors declare that they have no known competing financial interests or personal relationships that could have appeared to influence the work reported in this paper.

Acknowledgments

The authors would like to appreciate the financial support provided through EPSRC IAA 2022-23, UK Impact Builder Award and Innovate UK HyDEX project.

Data availability

Data will be made available on request.

References

- [1] Choudhury A, Chandra H, Arora A. Application of solid oxide fuel cell technology for power generation — A review. *Renew Sustain Energy Rev*, 2013;20:430–42.
- [2] Kupecki J. Off-design analysis of a micro-CHP unit with solid oxide fuel cells fed by DME. *Int J Hydrogen Energy* 2015;40(35):12009–22.
- [3] F. Baldi, L. Wang, M. Pérez-fortes, and F. Maréchal, “A Cogeneration System Based on Solid Oxide and Proton Exchange Membrane Fuel Cells With Hybrid Storage for Off-Grid Applications,” *Front. Energy Res.*, vol. 6, no. 139, 2019.
- [4] Ni M, Leung MKH, Leung DYC. Parametric study of solid oxide fuel cell performance. *Energy Convers Manag*, 2007;48(5):1525–35.
- [5] Connor PA, et al. Tailoring SOFC Electrode Microstructures for Improved Performance. *Adv Energy Mater*, 2018;8(1800120):1–20.
- [6] Ding D, Li X, Lai Y, Liu M. Enhancing SOFC cathode performance by surface modification through in filtration. *Energy Environ Sci*, 2014;7:552–75.
- [7] Tan L, Dong X, Chen C, Gong Z, Wang M. Diverse system layouts promising fine performance demonstration: A comprehensive review on present designs of SOFC-based energy systems for building applications. *Energy Convers Manag*, 2021;245: 114539.
- [8] Zhang L, Xing Y, Xu H, Wang H, Zhong J, Xuan J. Comparative study of solid oxide fuel cell combined heat and power system with Multi-Stage Exhaust Chemical Energy Recycling : Modeling, experiment and optimization. *Energy Convers Manag*, 2017;139:79–88.
- [9] Qu J, et al. Thermodynamic analysis and comprehensive system optimization of the near zero emission hybrid power based on SOFC-ICE integrated system fueled with ammonia. *Energy Convers Manag*, 2023;vol. 294, no. June:117553.
- [10] Chitsaz A, Sadeghi M, Sadeghi M, Ghanbarloo E. Exergoenvironmental comparison of internal reforming against external reforming in a cogeneration system based on solid oxide fuel cell using an evolutionary algorithm. *Energy* 2018;144:420–31.
- [11] Chen H, Yang C, Zhou N, Harun NF, Tucker D. “Performance Comparison of Internal and External Reforming for Hybrid SOFC-GT Applications by Using 1D Real-Time Fuel Cell,” in *Turbo Expo: Power for Land, Sea, and Air* 2019:1–6.
- [12] Cocco D. Comparative Performance Analysis of Internal and External Reforming of Methanol in SOFC-MGT Hybrid Power Plants. *J Eng Gas Turbines Power* 2007;129: 478–87.
- [13] Liese EA, Gemmen RS. Performance Comparison of Internal Reforming Against External Reforming in a Solid Oxide Fuel Cell , Gas Turbine. *J Eng Gas Turbines Power* 2005;127:86–90.
- [14] Authayanun S, Pornjarungsak T, Prukpraiapadung T. SOFC Running on Steam Reforming of Biogas: External and Internal Reforming. *Chem Eng Trans*, 2016;52: 361–6.
- [15] Liso V, Olesen AC, Nielsen MP, Kær SK. Performance comparison between partial oxidation and methane steam reforming processes for solid oxide fuel cell (SOFC) micro combined heat and power (CHP) system. *Energy* 2011;36(7):4216–26.
- [16] Zhang W, Croiset E. Simulation of a tubular solid oxide fuel cell stack using AspenPlus TM unit operation models. *Energy Convers Manag*, 2005;46:181–96.
- [17] Doherty W, Soc JE, Doherty W, Reynolds A, Kennedy D. Simulation of a Tubular Solid Oxide Fuel Cell Stack Operating on Biomass Syngas Using Aspen Plus. *J Electrochem Soc*, 2010;157:B975–81.
- [18] A. A. Ibrahim, “Chapter 3: Hydrogen Production from Light Hydrocarbons,” in *Advances In Hydrogen Generation Technologies*, 2018, p. 39.
- [19] L. Ma, “Hydrogen production from steam reforming of light hydrocarbons in an autothermic system,” 1995.
- [20] Speight JG. Gasification of Unconventional Feedstocks. *Gasif Unconv Feed* 2014;1: 1–191.
- [21] R. Luque and J. G. Speight, *Gasification for Synthetic Fuel Production: Fundamentals, Processes and Applications*. Gasif Synth Fuel Prod Fundam Process Appl, 2014.
- [22] Nguyen TH, et al. Partial oxidation of methane over NiO/La2O3 bifunctional catalyst II: Global kinetics of methane total oxidation, dry reforming and partial oxidation. *Appl Catal B Environ*, 2015;165:389–98.
- [23] J. Garche, C. K. Dyer, P. T. Moseley, Z. Ogumi, D. A. J. R. And, and Bruno, *Encyclopedia of electrochemical power sources*, 5th ed. Amsterdam, Boston: Academic Press : Imprint of Elsevier, 2009.
- [24] EG&G Services Parsons, *Fuel cell handbook*, 5th ed. 2000.
- [25] Amiri A, Tang S, Vijay P, Tadé MO. Planar solid oxide fuel cell modeling and optimization targeting the stack’s temperature gradient minimization. *Ind Eng Chem Res*, 2016;55(27):7446–55.
- [26] Amiri A, Vijay P, Tad MO, Ahmed K. Planar SOFC system modelling and simulation including a 3D stack module. *Int J Hydrogen Energy* 2016;41:2919–30.
- [27] Inui Y, Urata A, Ito N, Nakajima T, Tanaka T. Performance simulation of planar SOFC using mixed hydrogen and carbon monoxide gases as fuel. *Energy Convers Manag*, 2006;47(13–14):1738–47.
- [28] EG&G, “Technical Services I. Fuel cell handbook,” in *Choice Rev Online*, 26th ed., 1989, p. 6292.
- [29] J. B. Hansen, “Chapter 13: Direct Reforming Fuel Cells,” in *Fuel Cells: Technologies for Fuel Processing*, Elsevier, 2011, pp. 409–450.
- [30] J. Rostrup-Nielsen and J. B. Hansen, “Chapter 4: Steam Reforming for Fuel Cells,” in *Fuel Cells: Technologies for Fuel Processing*, Elsevier, 2011, pp. 49–71.
- [31] Sen F, Kasper T, Bergmann U, Hegner R, Atakan B. Partial oxidation of methane at elevated pressures and effects of propene and ethane as additive: Experiment and simulation. *Zeitschrift fur Phys Chemie* 2015;229(6):955–76.
- [32] York APE, Xiao T, Green MLH. Brief overview of the partial oxidation of methane to synthesis gas. *Top Catal*, 2003;22(3–4):345–58.
- [33] Fleys M, Shan W, Simon Y, Marquaire PM. Detailed kinetic study of the partial oxidation of methane over La2O3 catalyst. Part I: Experimental results. *Ind Eng Chem Res*, 2007;46(4):1063–8.
- [34] Rabe S, Truong TB, Vogel F. Low temperature catalytic partial oxidation of methane for gas-to-liquids applications. *Appl Catal A Gen*, 2005;292(1–2):177–88.
- [35] Peymani M, Alavi SM, Rezaei M. Synthesis gas production by catalytic partial oxidation of methane, ethane and propane on mesoporous nanocrystalline Ni/ Al2O3 catalysts. *Int J Hydrogen Energy* 2016;41(42):19057–69.
- [36] Oni AO, Anaya K, Giwa T, Di Lullo G, Kumar A. Comparative assessment of blue hydrogen from steam methane reforming, autothermal reforming, and natural gas decomposition technologies for natural gas-producing regions. *Energy Convers Manag*, 2022;254:115245.
- [37] Karakaya M, Ilsen Onsan Z, Avci AK. Microchannel autothermal reforming of methane to synthesis gas. *Top Catal*, 2013;56(18–20):1716–23.
- [38] Ayabe S, et al. Catalytic autothermal reforming of methane and propane over supported metal catalysts. *Appl Catal A Gen*, 2003;241(1–2):261–9.
- [39] Chiesa P. “Advanced technologies for syngas and hydrogen (H2) production from fossil-fuel feedstocks in power plants,” in *Advanced Power Plant Materials. Design and Technology* 2010:383–411.
- [40] M. A. Reese, “High pressure autothermal reforming in low oxygen environments,” 2008.
- [41] Cavalcante MHS, et al. Autothermal Reforming of Methane: A Thermodynamic Study on the Use of Air and Pure Oxygen as Oxidizing Agents in Isothermal and Adiabatic Systems. *Methane* 2023;2(4):389–403.